Climate Dynamics (2024) 62:3321–3336
https://doi.org/10.1007/s00382-023-07067-0

ORIGINAL ARTICLE

A quasi-geostrophic analysis of summertime southern African linear-regime westerly waves

Thando Ndarana[1] · Tsholanang S. Rammopo[1] · Mary-Jane M. Bopape[1,2] · Neil C. G. Hart[3] · Chris J. C. Reason[4] · Hector Chikoore[5]

Received: 10 July 2023 / Accepted: 9 December 2023 / Published online: 18 January 2024

Abstract

Linear-regime westerly waves that propagate across the South African domain are often linked to well-known rainfall producing systems such as tropical temperate troughs and synoptic scale tropical low-pressure systems, and ridging South Atlantic Ocean anticyclones at the surface. It is accepted that the baroclinic waves that propagate across the domain provide the lifting mechanism that causes the required vertical motion for rainfall to occur. This study shows that there exists a jet streak embedded in these waves that is located downstream of the trough axis, to the east of which vertically upward motion is expected to occur. The entrance of the jet streak passes just south of the country, as the waves propagate past the domain. The study further shows that for this class of waves, the vertical motion that causes rainfall to occur is induced by the thermally direct transverse ageostrophic circulation that is located at this jet entrance. This is instead of the conventional upper air divergence that is located at the inflection point east of the trough axis. Using a method of decomposing the Q-vector into its transverse (Q_n) and shear (Q_s) components, the divergence fields of which are used to decompose the vertical motion into the corresponding components, i.e ω_n and ω_s, respectively; it was shown that the vertical motion over South Africa is explained more by the former than the latter. Therefore, the uplift over the country and that located at the infection point east of the trough are dynamically distinct processes. Taking the limitations of the quasi-geostrophic framework into consideration, the study concludes that during the passage of linear-regime waves vertical motion that might lead to rainfall is caused by the circulation at the jet entrance and not the divergence in the baroclinic wave.

Keywords Westerly wave · Jet streak · Q-vector

1 Introduction

As southern Africa is situated on the subtropical belt, its summer weather is, to a degree, influenced by disturbances in the extra-tropical westerlies. Few studies have had a primary focus on wave dynamics over southern Africa, an exception being Kelbe (1988) for example, with most focusing on the well-established role of these waves in regional rainfall (Tyson and Preston-Whyte 2002). Chief among these rainfall producing processes are tropical-temperate troughs

✉ Thando Ndarana
thando.ndarana@up.ac.za

Tsholanang S. Rammopo
rammopo.ts@tuks.co.za

Mary-Jane M. Bopape
mm.bopape@saeon.nrf.ac.za

Neil C. G. Hart
neil.hart@ouce.ox.ac.uk

Chris J. C. Reason
chris.reason@uct.ac.za

Hector Chikoore
hector.chikoore@ul.ac.za

1 Department of Geography, Geoinformatcs and Meteorology, University of Pretoria, Hatfield, South Africa

2 South African Environmental Observation Network, Colbyn, South Africa

3 School of Geography and the Environment, University of Oxford, Oxford, UK

4 Department of Oceanography, University of Cape Town, Cape Town, South Africa

5 Department of Geography and Environmental Studies, University of Limpopo, Sovenga, South Africa

(TTTs), characterised by tropical-extratropical cloud bands oriented diagonally northwest-southeast across southern Africa (Harrison 1984; Hart et al. 2023). Observational and modelling studies show that TTTs are typically associated with upper-tropospheric westerly waves and that wave phasing may be important for the persistence of rainfall over the subcontinent (Harangozo and Harrison 1983; Hart et al. 2010; Vigaud et al. 2012; Macron et al. 2014). Hart et al. (2023) found that these TTTs peak in November over the region consistent with the notion that westerly waves influence rainfall more strongly during early summer (D'Abreton and Lindesay 1993).

The importance of westerly waves is not limited to the TTTs. Synoptic-scale ridging of the South Atlantic high (SAOH) pressure system eastward across the southern coast of Africa is crucial to coastal rainfall and regional moisture fluxes (Ndarana et al. 2021a, b) and is associated with westerly wave dynamics aloft (Ndarana et al. 2022). Further equatorward, Kuete et al. (2020) found that westerly waves may be linked to pulsing of the African Easterly Jet-South. Viljoen et al. (2023) suggested that the westerly wave is also associated with a tropical cyclone-like low pressure systems found over land, which they refer to as the Africáne.

But, it is westerly waves that venture into non-linear regimes and break that have received the most detailed dynamical analyses in the literature. Wave breaking processes are most clearly seen in isentropic potential vorticity (PV) fields and is signalled by the PV contours becoming irreversibly deformed and turning back on themselves so that the PV gradient becomes negative (McIntyre and Palmer 1983; Thorncroft et al. 1993; Peters and Waugh 1996). When an isolated positive PV anomaly is found in the trough as a result of the wave breaking, a closed cyclonic circulation is then induced (Hoskins et al. 1985) and a cut-off low (COL) pressure system forms, which by definition is a closed circulation that has detached from the main westerlies (Palmén 1949; Palmén and Newton 1969). Numerous studies have considered COLs in the South African domain (Taljaard 1985; Fuenzalida et al. 2005; Pinheiro et al. 2017) and assessed their interannual variability (Singleton and Reason 2007a; Favre et al. 2012, 2013) due to the extreme rainfall and winds associated with these systems when they extend to the surface (Singleton and Reason 2006; Engelbrecht et al. 2015; Barnes et al. 2021a, b, 2022; Thoithi et al. 2022) due to depth of the associated PV anomaly (Barnes et al. 2022). At times a surface meso-low (Singleton and Reason 2007b; Thoithi et al. 2022) may develop during COLs, which may lead to strong onshore moisture fluxes (Thoithi et al. 2022), which may also be assisted by the long fetch from further into the South Indian Ocean, possibly caused by Type-S ridging events (Ndarana et al. 2022). Combining the moisture presence over the land with the large-scale upper-level divergence that is induced in strongly curved flow fields during wave breaking is often invoked to explain extreme rainfall associated with COLs and other weather systems such as TTTs (e.g. Hart et al. 2010).

This extensive analysis of non-linear wave breaking regimes associated with weather extremes has diagnosed the key role of downstream development (Gan and Piva 2013, 2016; Ndarana et al. 2021a, b; Pinheiro et al. 2022; Ndarana et al. 2023), which is largely facilitated by the strength of the jet streak located immediately upstream of ridge to the west of the main trough axis. Ndarana et al. (2023) diagnosed that during ridging SAOH events which are associated with a COL aloft, the upstream jet streak is stronger than the one located downstream of the trough axis. This configuration then increases strain rates so that the waves may break (Nakamura and Plumb 1994; Akahori and Yoden 1997). Why some waves in the South African domain enter non-linear regimes and others remain in more linear regimes is still an open question. However, Ndarana et al. (2023) showed that baroclinic conversion observed during the latter is less intense than in the case of former, meaning that when COLs (in general wave breaking) do not occur it is suppressed. A working hypothesis is that the barotropic governor mechanism (James and Gray 1986; James 1987) might be responsible for this. Moon and Feldstein (2009) showed that it leads to weaker upward fluxes of wave activity during the initial states of their weak barotropic wave life cycle case, which might explain the weaker increase in eddy kinetic energy generation during linear-regime waves in the South African domain (Ndarana et al. 2023).

It is clear from these studies that westerly waves in more linear regimes may play a substantial role in South African summer rainfall but are under studied. Indeed the majority of westerly disturbances do not enter a non-linear wave-breaking regime. For example in the case of ridging highs, Ivanciu et al. (2022) showed that only 44% of them were associated with wave breaking aloft. The dynamics associated with these linear waves are important to understand, especially as there may be different processes at play as compared to non-linear regime waves. As will be shown in this paper, the location of the upstream jet streaks west of the main wave trough might have a profound influence on the atmospheric dynamics influencing the country because they can be oriented such that jet entrances overlie the country as the disturbances propagate past. The conventional wisdom is that the dynamical ascent found over southern Africa during the passage of a westerly trough is caused by upper air divergence east of it. However, the presence of the jet streak and the location of its entrance could invoke a thermally direct transverse circulation, as described for straight zonal jets (Keyser and Shapiro 1986) and jet streaks greatly influenced by curvature (Moore and VanKnowe 1992). This might mean that vertical ascent over the country is caused by this transverse circulation, rather than the Dines compensation mechanism. Studies that consider such dynamics for linear-regime waves issue are missing in the literature for the region. In this respect, the research question raised in this study is: What is the relative importance of vertical motion associated with the jet entrance compared to that associated with upper-level divergence embedded in the wave trough of a westerly wave?

The rest of the paper is structured as follows: In the next session the data and methods are outlined, including the quasi-geostrophic diagnostics used in the study. In Sect. 3 the results are presented and the concluding remarks are provided in Sect. 4.

2 Data and methods

2.1 Data

The variables represented in the mathematical diagnostics that describe the dynamical processes considered in this study are obtained from the Fifth Generation European Centre for Medium Range Weather Forecasts Reanalysis (ERA5, Hersbach et al. 2020) from 1979 to 2020. Because westerly waves and jet streaks are synoptic scale processes ($\sim 10^6$ m, Holton and Hakim 2014); a grid spacing of 2.5°×2.5°, which translates to about 278 km × 278 km, and the 6 hly time intervals are deemed sufficient to resolve all processes of relevance to the study. The basic meteorological fields used in the calculations, namely the three dimensional flow ($\mathbf{u} = u\mathbf{i} + v\mathbf{j} + \omega\mathbf{k}$), the geopotential ($\phi$) and temperature ($t$) are downloaded at standard pressure levels, namely 1000, 925, 850, 700, 500, 400, 300, 250, 200, 150, 100, 70, 50, 30, 20 10 hPa. The mean sea level pressure (MSLP) fields are available at a single level.

2.2 Methods

2.2.1 Identifying instances of linear westerly wave and ridging high co-occurrence

The subject of this study is the linear westerly wave, which as noted in Sect. 1, may be associated with rainfall over the southern and south-eastern coastal parts of South Africa. One of the ingredients for rainfall is the presence of moisture over land, which in the case of the westerly wave, originates from the South West Indian Ocean and is transported by the onshore flow that is induced by the ridging process (Cook et al. 2004; Dyson 2015; Ndarana et al. 2021a, b), as noted in the Introduction. For this reason, we first identify ridging high events and focus on the December to February (DJF) months using an objective method whose full description is outlined in Ndarana et al. (2018). For ease of reference, we provide a brief description of it here. The algorithm is composed of three steps, the first of which is to objectively identify closed MSLP contours in the domain bounded by the 40°W and 60°E latitude lines. Thereafter concentric closed contours are grouped together such that the MSLP increases inward. This captures the SAOH pressure system. The grouping of the contours is the second step and in the third one we require that the outermost contour extends east across the 25°E so that by definition, a ridging high has occurred. To identify individual ridging events we require that this eastward extension condition be met at consecutive time steps, without breaks in between. If a break is identified, then we deem that instant at the end an event. So, the number of 6-h time steps from the first time that the extension across the 25°E occurs to this cut-off defines the duration of the ridging events.

To address the objectives of this study, we capture instances when ridging events occur without breaking waves by objectively checking if two days prior, during, and two days after the cessation of a ridging event with in the confines of the 40°W and 60°E domain there is no potential vorticity overturning on the 350, 340 and 330 K isentropic surfaces. If a ridging event is found to co-occur with a breaking wave signal, then it is removed from the original database. This is aimed at reducing the possibility of non-linear waves in the domain so that ridging high cases will only occur with waves that comply with linear wave theory propagating across the South African domain remain for analysis.

A total of 164 such ridging high events were identified and were used to create composite fields. Composite analysis is a simple but powerful method that is commonly used in observation studies to establish dynamical processes associated with weather systems. To create the composite fields, all the basic and derived variables on the dates and hours of the first time that ridging events are identified and then averaged. This constitutes composite mean fields for the time lag $t = 0$ h. This is process is repeated for t = ±6, ±12,.., ±48 hr time steps. Compositing removes the variations and differences between events, whilst highlighting the robust characteristics and features of the weather system processes and where relevant, the statistical significance is established employing the method of Brown and Hall (1999).

2.2.2 Diagnostics

It is instructive for this study to review the quasi-geostrophic diagnostics associated with jet streak transverse ageostrophic circulations, which we discuss here in the context of an idealised baroclinic wave shown in Fig. 1. The schematic and accompanying discussion draw from Keyser and Shapiro (1986), Sanders and Hoskins (1990), Simmonds and Keay (2000), Lim et al. (1991) and Martin (2006) and including only processes that are relevant to the study. The right hand side of the traditional adiabatic ω-equation in isobaric coordinates

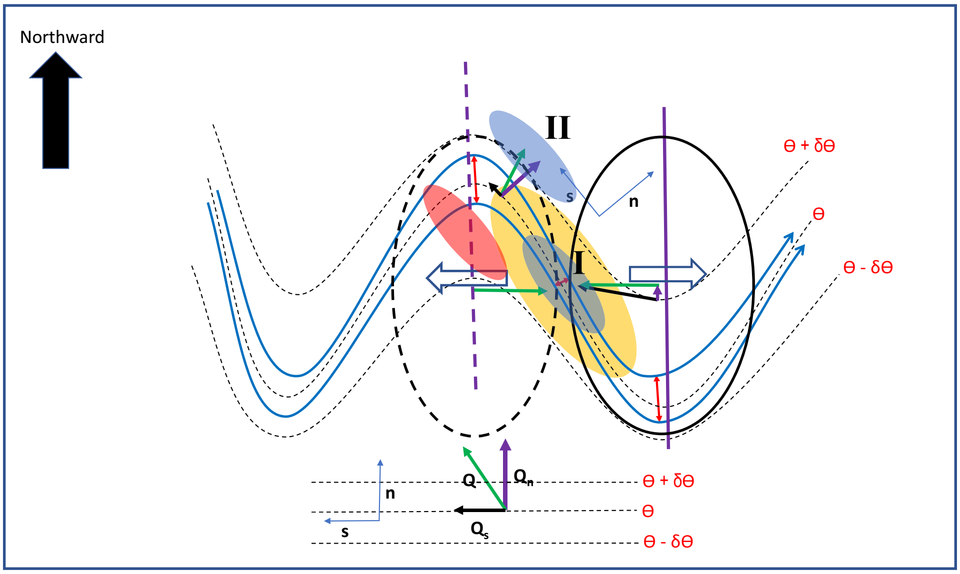

Fig. 1 A schematic of a jet streak or baroclinic zone (yellow shading) embedded on a baroclinic wave between an upstream trough axis (dashed purple straight line) and downstream ridge (solid purple straight line) axes. The thick blues solid curves represent the upper level isohypses and the thin black dashed curves represent the isentropes at the pressure level as the isohypse. The isentrope values increase northward (thick black arrow at the top left of the figure). The separation between the isohypse at the jet entrance and exit represent the confluent and diffluent flow (as indicated by the size of the red double arrow near the axes compared to the inflection point). The green arrows represent the **Q** vectors and the black and purple arrows represent their components, $\mathbf{Q}_s$ and $\mathbf{Q}_n$, in the direction of the unit vectors **s** and **n**, respectively. The open arrows represent the diverging ageostrophic flow and located at in the middle of the negative (dashed oval shape) and positive (solid oval shape) geopotential anomalies. Two areas of ascent are labelled I and II. [Adapted from Fig 4a in Keyser and Shapiro (1986), Fig 6 in Lim et al. (1991), Figs 4 and 5a in Sanders and Hoskins (1990), Fig 2 in Martin (2006)]

comprises two terms; namely the vertical divergence of the geostrophic relative vorticity advection by the geostrophic flow and the Laplacian of the geostrophic temperature advection (see Holton and Hakim 2014). The main drawback of this form of the equation is that these two terms tend to cancel each other, which prompted Hoskins et al. (1978) to seek an alternative form of it that expresses its right hand side succinctly as the negative of twice the divergence of the so-called **Q**-vector. Assuming a constant Coriolis parameter, f_o, calculated at a reference latitude $\phi_o = 45°S$, the ω-equation then takes the form

$$L\omega_{qg} = -2\nabla \cdot \mathbf{Q} \tag{1}$$

where ω_{qg} is the quasi-geostrophic vertical motion, L is the linear differential operator defined as $L = \sigma\nabla^2 + f_o^2\partial_p^2$ (Park et al. 2021) and, as in Martin (2006), **Q** is defined by

$$\mathbf{Q} = -f_o\gamma\left[\left(\partial_x\mathbf{V}_g \cdot \nabla\theta\right)\mathbf{i} + \left(\partial_y\mathbf{V}_g \cdot \nabla\theta\right)\mathbf{j}\right]. \tag{2}$$

In these equations, σ is the static stability, given explicitly by $\sigma = (-RT_o)(p_o\theta)^{-1}\partial_p\theta$ where T_o and θ_o are, respectively the averaged temperature and potential temperature over the domain of interest and the quantity $\gamma = (Rp_o)(f_o^{-1})(p_op^{-1})^{c_v/c_p}$. Here R is the ideal gas constant, p_o is the standard pressure level taken to be 1000 hPa, and c_v (c_p) is the specific heat capacity at constant volume (pressure). Because f_o is constant, the geostrophic flow in Eq. (2) is therefore non-divergent so that ω_{qg} is induced purely by the ageostrophic component of the flow, as required by the isobaric continuity equation.

The term $-2\nabla \cdot \mathbf{Q}$ is a forcing in Eq. (1) and given the fact that $L\omega_{qg} \propto -\omega_{qg}$, then areas of $\nabla \cdot \mathbf{Q} < 0$ are associated with $\omega_{qg} < 0$. In Fig. 1, **Q** is represented by the green arrows, which converge at the inflection point of the wave, east of the trough axis (Sanders and Hoskins 1990; Simmonds and Keay 2000; Holton and Hakim 2014). This is also an area of upper air divergence, as indicated by the open arrows that are pointing in opposite directions, representing the behaviour of the ageostrophic flow at the inflection point of a baroclinic wave (Lim et al. 1991). The resulting vertical ascent is represented by the blue oval shape and marked I in Fig. 1. In the geographical context of South Africa, this area of vertical ascent would generally be located in the extratropics, except perhaps in cases of COLs and deep troughs that have a northwest/southeast orientation.

Figure 1 also shows a second area of vertical ascent represented by the blue oval shape near the top of the wave, marked II. It is found on the cyclonic confluent side of the jet streak; which is represented by the yellow oval shape, also indicated by the converging thick blue contours that represent the upper level isohypses. On the cyclonic confluent side of the jet entrance there is convergence of ageostrophic wind downward motion (red oval shape), which of course would complete the thermally direct transverse circulation (Keyser and Shapiro 1986). Here, the **Q** vectors are nearly perpendicular to the isentropic contours and point towards warmer temperatures (Sanders and Hoskins 1990; Simmonds and Keay 2000; Holton and Hakim 2014).

Keyser et al. (1992) showed that vertical motion may be partitioned into along- and cross-isentrope components, which is achieved by first resolving **Q** into a component that is normal to the isentropes, denoted by $\mathbf{Q}_n$ and also referred to as the transverse component and another that is tangential to them, $\mathbf{Q}_s$, along unit vectors **n** and **s**, respectively. $\mathbf{Q}_s$ is also called the shearwise component. The version of diagnostics used in this study is that outlined in Martin (2006) and Park et al. (2021). In those studies, the unit vector **n** is chosen such that it points in the direction of increasing θ values and normal to the isentropic contours, that is, in the direction in which $\nabla\theta$ points, so that it may be defined as $\mathbf{n} = (|\nabla\theta|^{-1})\nabla\theta$ and the tangential unit vector **s** is rotated 90° to the left of direction of **n**, and it is therefore $\mathbf{s} = \mathbf{k} \times \mathbf{n}$. The transverse and shearwise components of **Q** may then be explicitly expressed as $\mathbf{Q}_n = (\mathbf{Q} \cdot \mathbf{n})\mathbf{n}$ and $\mathbf{Q}_s = (\mathbf{Q} \cdot \mathbf{s})\mathbf{s}$ and represented by the green, purple and black arrows, respectively in Fig. 1. On the basis of this decomposition of **Q**, the quasi-geostrophic vertical motion may then be partitioned using

$$L\omega_n = -2\nabla \cdot \mathbf{Q}_n \tag{3}$$

and

$$L\omega_s = -2\nabla \cdot \mathbf{Q}_s \tag{4}$$

In the schematic shown in Fig. 1, the orientation of **Q** on the anticyclonic confluent side of the jet streak is such that it tends to be more cross-isentropical (Sanders and Hoskins 1990; Simmonds and Keay 2000) so that $|\mathbf{Q}_n|$ tends to be larger than $|\mathbf{Q}_s|$. The opposite holds in the vicinity of the inflection point. This qualitative observation is consistent with Keyser et al. (1992)'s and Martin (2006)'s characterisation that $-2\nabla \cdot \mathbf{Q}_n$ is a forcing of the transverse vertical motion ω_n (ascent II in Fig. 1), whereas $-2\nabla \cdot \mathbf{Q}_s$ is a forcing on the shearwise vertical motion ω_s (ascent I in Fig. 1), as inferred from Sanders and Hoskins (1990). Note that ω_n may also be found across the frontal region and it is expected to form a band like structure, whilst ω_s fields are circular; which Keyser et al. (1992) referred to as wave scale. Park et al. (2021) found this to be the case in their diagnosis of heavy rainfall events over the South Korean peninsula.

To quantitatively show that the processes that lead to ascent II which occurs over South Africa and are different from those that lead to ascent I in the extra-tropics, Eqs. (1), (3) and (4) are then inverted by means of successive over-relaxation using the method of Park et al. (2021) to obtain the ω_{qg}, ω_n and ω_s fields to directly link these vertical velocity fields with the forcings shown on the right hand side of the equations. All the fields calculated from these diagnostics are presented as composites in the following sections.

3 Results

3.1 Linear wave propagation

We first consider the propagation of the westerly waves, as defined above, that affect the South African domain from a wave packet perspective, to provide a broad overview of their propagation characteristics. Figure 2 shows a Hovmöller plot of 250 hPa z' fields averaged between 60°S and 35°S, with the individual eddies of the wave packet labelled with Roman numerals I–V. These were calculated by subtracting the 31-day mean centred on the $t = 0$ hrs from the total fields. The black and red dashed lines are drawn at 10°E and 35°E, respectively, to estimate the location of the South African domain. The Hovmöller shows that the first trough (marked I) appears just east of 150° W at about $t = -186$ h and it is associated with ridge (marked II), which appears at about $t = -96$ h. A secondary trough-ridge system develops in the South Atlantic Ocean and it is this secondary

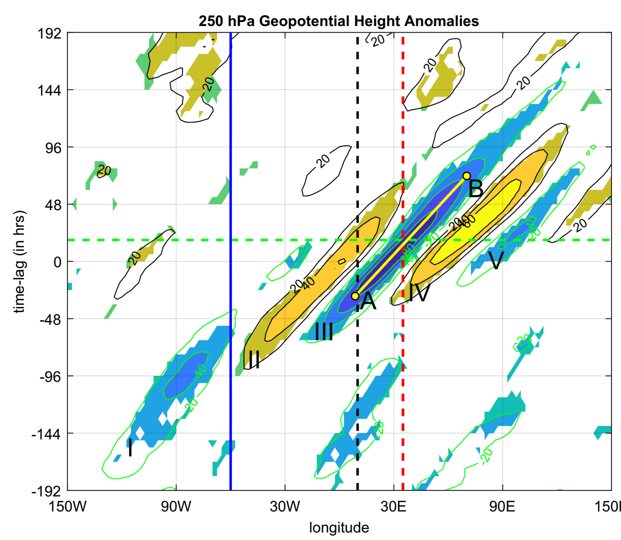

Fig. 2 Hovmöller of composite produced by averaging 250 hPa geopotential height anomalies from 60°S to 35°S and plotted in 4 gpm intervals. The black and green contours represent positive and negative values, respectively. The blue solid line marks 60°W. The dashed black and red lines mark the 10°E and 35°E, respectively, mark the South African domain and eddies are labelled I–V. The yellow line AB approximate the trough axis of eddy III. The shaded areas indicate where the composite geopotential height anomalies are significant at the 95% confidence level

development that eventually impacts the South African domain, as indicated by the trough axis (estimated yellow line AB) crossing the 10°E line at about $t = -24$ hrs.

Several studies (e.g. Jones and Simmonds 1993; Sinclair 1995; Simmonds and Keay 2000; Mendes et al. 2007; Reboita et al. 2010, 2019; Crespo et al. 2021) have identified preferred areas of cyclogenesis, just off the eastern coast of South America close to Drake passage as well as across it and westward into the eastern South Pacific Ocean; and in the South Atlantic Ocean, to the southwest of the African mainland. The linear westerly waves that eventually propagate into the South African domain appear to be developing from these, according to Fig. 2. They are mainly characterised by two jet streaks, the downstream of which is stronger, so that the one upstream does not lead to wave breaking and COLs. Previous studies (e.g. Ndarana and Waugh 2010; Reyers and Shao 2019; Ndarana et al. 2023) showed that the upstream jet streak would need to be much stronger for this to take place, regardless of region, as Reyers and Shao (2019) found this to be the case in the eastern South Pacific Ocean and South American region and Ndarana et al. (2023) showed it for the South African sector.

Figure 3 shows composites of the westerly waves produced by using the occurrence of ridging highs as the guiding centre, that is $t = 0$ h which corresponds to the first instance that ridging was identified, as explained in Sect. 2. The dashed (solid) thin contours represent the negative (positive) geopotential height anomalies at 250 hPa. The shaded

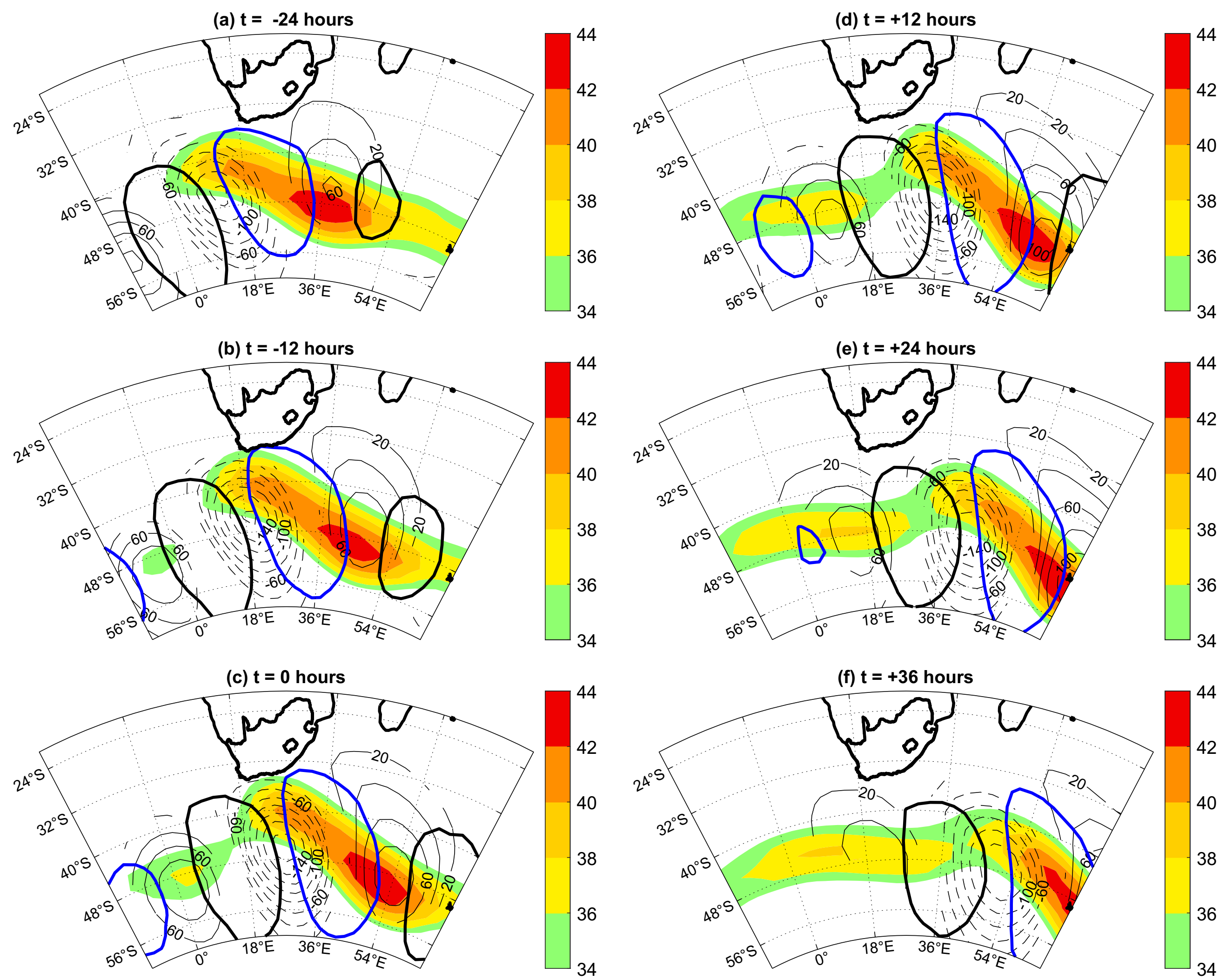

Fig. 3 Composite evolution of the zonal isotachs (shaded) plotted from 34 m s^{-1}. This solid and dashed thin black contours represent the positive and negative geopotential height anomalies, respectively, plotted in 20 gpm contour intervals. Only anomalies that significant at the 95% confidence level are shown. The thick blue and black closed curves represent the $v' = -6$ and 6 m s^{-1} values, respectively. The composite fields are shown from (**a**) $t = -30$ to (**f**) $t = +18$ h in 6 hly intervals. All the fields are plotted at the 250 hPa level

region represents composite mean 250 hPa zonal isotachs field, indicating the location and orientation of the frontal zone as the baroclinic wave evolves. It is well known that at the top of the trough axis, which is located at the top of the wave close to the mainland, the flow is subgeostrophic, and supergeostrophic at the bottom of the ridge (Orlanski and Sheldon (1995)). For the composites shown in Fig. 3, the subgeostrophic flow is associated with the jet entrance. The supergeostrophic flow in ridge is caused by the fact that across the ridge axis located in the region of maximum $z' > 0$ gpm, just before the jet exit.

The composite evolution of the fields shows that the jet streak starts off oriented quasi-zonally and then the one downstream attains a northwest/southeast orientation as the trough axis enters the South African domain, so that its entrance moves towards the land, touches it and then propagates away, as though it is reflected out of the domain. As the downstream jet streak leaves the South African domain, the upstream jet streak exit regions crosses the 10°E latitude line. This orientation and evolution of the downstream jet streak has profound implications for vertical ascent over South Africa, which will be discussed next.

3.2 Jet streak and baroclinic wave circulations

Section 3.1 highlighted the downstream jet streak and its orientation relative to the South African mainland as the westerly wave propagates across the domain. As it is common practice in the study of observed upper level frontal systems (e.g. Martin 2014), Fig. 4 presents a tropospheric cross-section through the 25°E longitude line, with the arrows representing the transverse circulation $v_a\mathbf{j} - \omega\mathbf{k}$ vector field and the shading representing $\partial_y v_a$. The well-known thermally direct circulation (Keyser and Shapiro 1986) is evident (Fig 4a), with vertically upward motion north of 35°S; placing it over South Africa, which is estimated to be located between the black and red dashed lines. Even though this is not a west-east oriented straight jet, we assume cross-front geostrophy as in Keyser and Shapiro (1986) so that the continuity equation then becomes $\partial_y v_a + \partial_p \omega = 0$ because $|\partial_x u_a| \ll |\partial_y v_a|$. Fig 4a shows that at the lower levels we have $\partial_y v_a < 0$ over South Africa, with $\partial_y v_a > 0$ aloft, so that the rising motion observed there occurs as a result of mass conservation. The flow then rotates in a thermally direct fashion, so that there is descent in the extra-tropics on the poleward side of the jet streak core. This descending motion is supported by the $\partial_y v_a < 0$ field in the extra-tropical upper troposphere and $\partial_y v_a > 0$ at the lower levels.

In Fig. 3, it is clear that the weaker upstream jet streak enters the South African sector as the downstream one exits it, so that there is no overturning of the geopotential height (and indeed potential vorticity) vorticity contours, as noted in Sect. 3.1. Note Fig. 4b shows that the relation $\partial_y v_a + \partial_p \omega = 0$ now fails over South Africa where downward motion is observed at the lower levels, but still holds in the extratropics; where there is a thermally indirect circulation at the exit of the second jet streak, as expected from theory (Keyser and Shapiro 1986). The weak character of the upstream jet streak, also means that the transverse circulation it induces as it crosses the 10°E latitude line will be

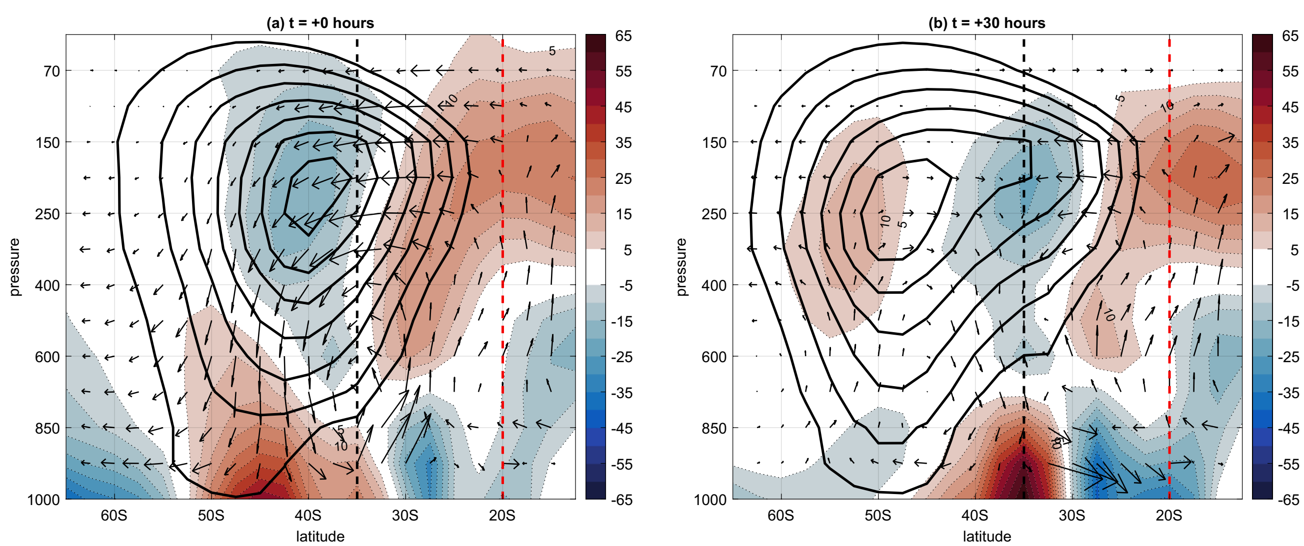

Fig. 4 Composites vertical cross-sections of the troposphere through the 25°E longitude line of the **a** downstream and **b** upstream jet streaks at $t = +6$ h and $t = +30$ h, respectively, represented by the thick black contours. The zonal isotachs, represented by the thick black contours, are plotted at 5 m s^{-1}. The shading represents the diagnostic $\partial_y v_a$, plotted at 10^6 s^{-1}. The arrows represent the transverse circulation $v_a\mathbf{j}$ - $\omega\mathbf{k}$. The black and red dashed lines estimate the location South Africa

weak and is apparently too far south to have an impact over the South African mainland.

It follows from the discussion of Fig. 4 that the vertically upward motion may be associated with the dynamics of the jet streak, rather than the upper level divergence east of the upper air trough axis that is strongest at the inflection point as shown schematically in Fig. 1 (Lim et al. 1991). The left panels of Fig. 5 present composites of the ω field at 700 hPa, which is an approximated level of non-divergence inferred from Fig. 4a. Note that these fields are smoothed by means of a 9-point spatial average to remove small scale disturbances. Figure 5a–c show that the composite vertical motion observed for $t = -24$, 0 and + 24 h over South Africa as the trough axis propagates through the domain is geographically linked to that which occurs in the extra-tropics. The sequence of events in these panels shows that the $\omega < 0$ that is observed prior to the westerly trough propagating across the 10°E latitude line is progressively replaced by $\omega > 0$ across the southern and southeastern coasts of South Africa, as the wave propagates past the domain.

Whilst Fig. 5a, b suggest that the vertical motion observed over the mainland appears to be an extension of the extratropical field, we propose here that these two fields manifest from very different dynamical processes. The first piece of the argument is presented above, which suggested that the transverse circulation of the downstream jet entrance is responsible for vertical uplift in

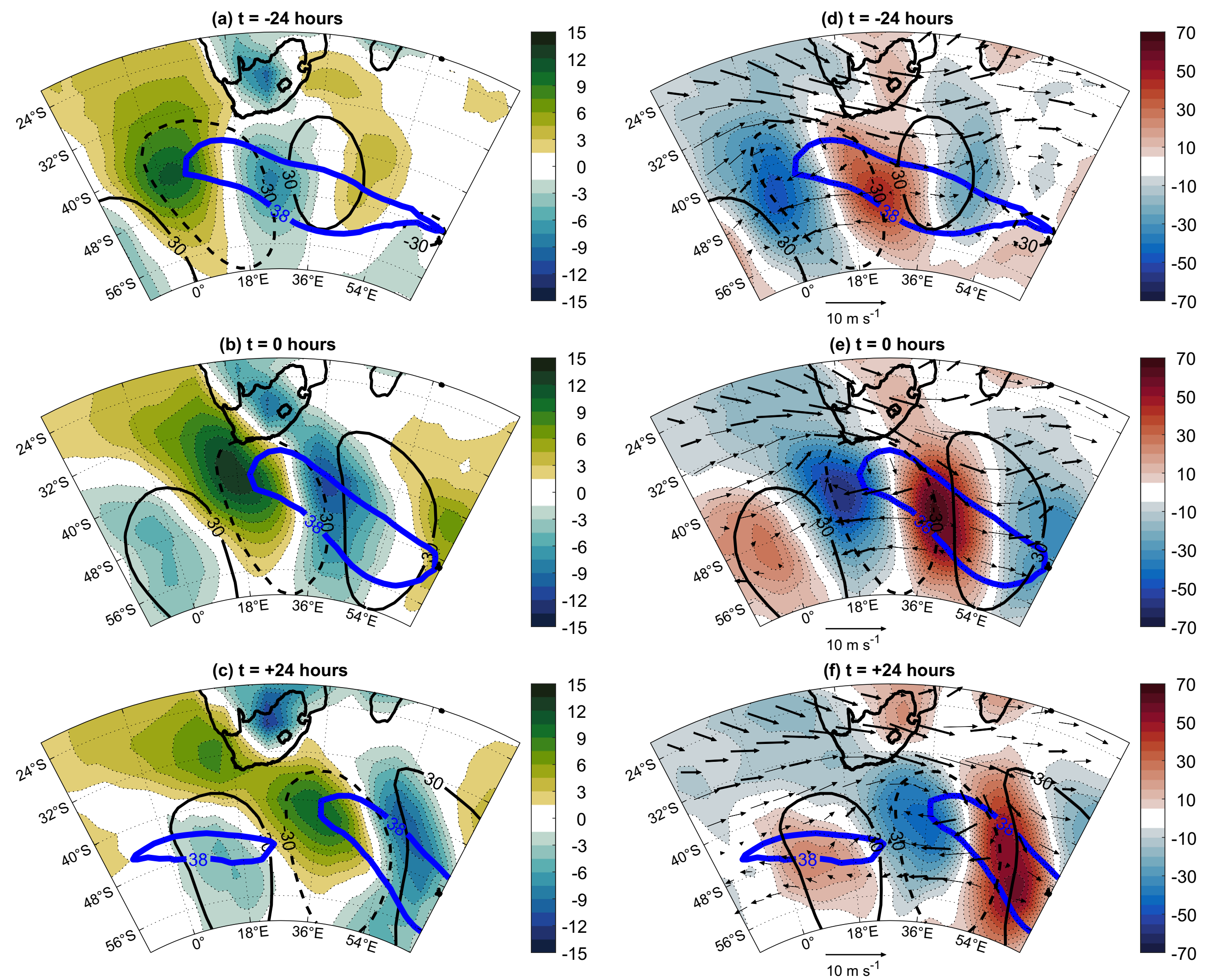

Fig. 5 The left panels show composites of ω at 700 hPa (shaded) plotted in 10^2Pa s^{-1} and the right panels show $\nabla \cdot \mathbf{v}_a$ (shaded) plotted in 10^7 s^{-1} and the $\mathbf{v_a}$ flow field (black arrows) both plotted at the 250 hPa isobaric surface. The thicker black arrows represent the ageostrophic flow that is significant at the 95% confidence level. In all panels, the thick blue contour represent the 38 m s^{-1} 250 hPa isotach to highlight the jet streak in Fig. 2 and the thinner solid (dashed) black closed curves are + 30 (- 30) gpm 250 hPa geopotential anomalies. The (**a**, **d**) top, (**b**, **e**) middle and (**c**, **f**) bottom panels are times lags at t = - 24 h, 0 h and + 24 h respectively

South Africa, whilst the extra-tropical is associated with the upper level ageostrophic divergence of the baroclinic wave (Lim et al. 1991).

To support this hypothesis we consider the ageostrophic flow and its divergence field plotted at the 250 hPa level and shown on the right panels of Fig. 5. Its structure over subtropical southern Africa is different from that which is observed in the extra-tropics. In the case of the former, it is diffluent so that the divergence field is predominantly caused by $\partial_y v_a$, which is consistent with the cross-front geostrophy assumption made earlier. In the extra-tropics the divergence field is dominated by the term $\partial_x u_a$ because the ageostrophic flow is zonal in the middle of the eddies (Fig. 5a, e, f; see also the schematic in Fig. 1; Lim et al. 1991). This suggests then that the two divergence fields do indeed manifest from different dynamical processes, so that the vertical motion fields they induce are dynamically distinct. In the next section this distinction will be shown by means of quasi-geostrophic diagnostics.

3.3 The Q-vector forcing

The qualitative argument presented above will now be supported by means of quasi-geostrophic diagnostics reviewed

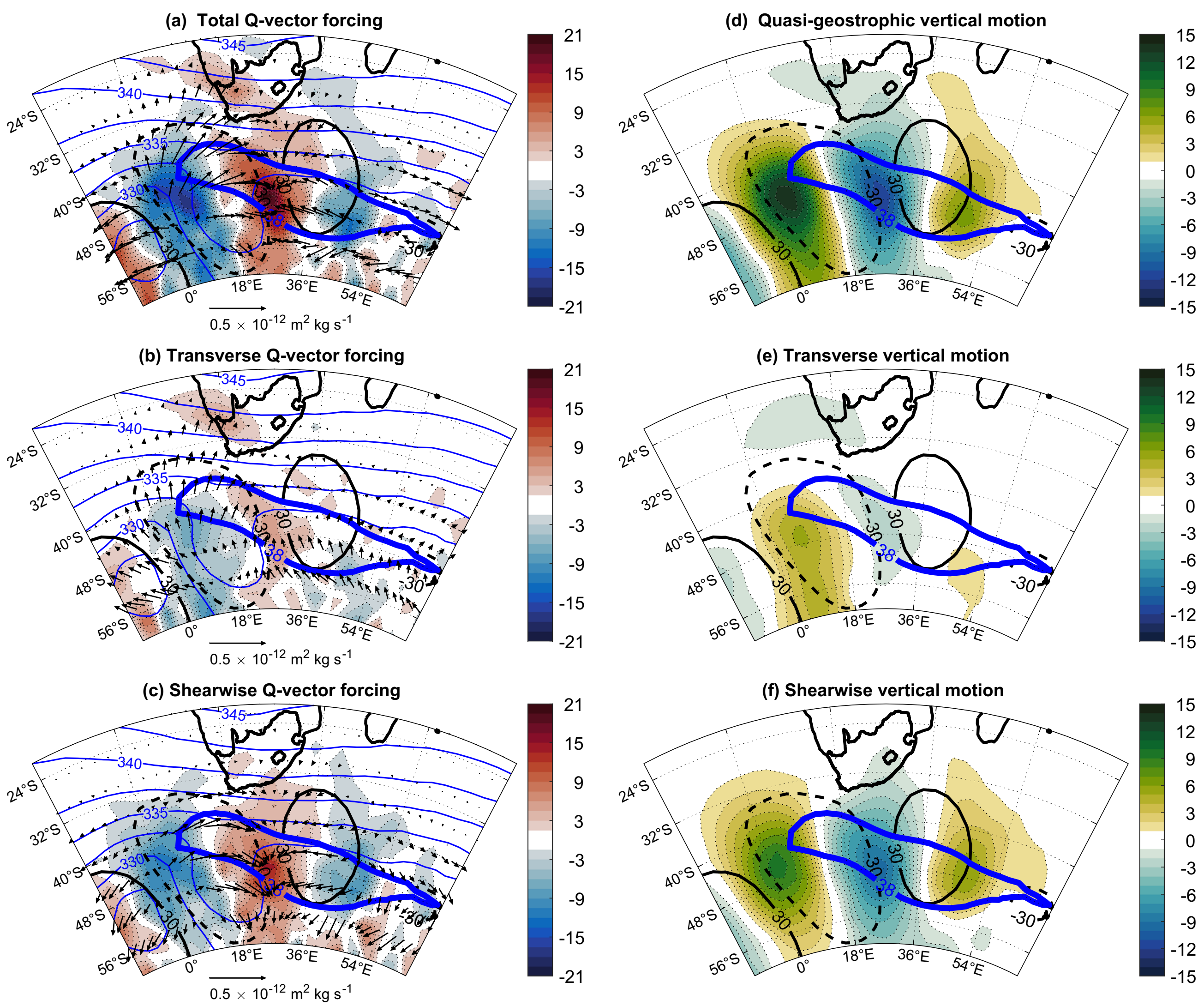

Fig. 6 Left panels show composites of 700 hPa Q-vectors (black arrows) and Q-vector forcing (shading) and right panels show the vertical motion (shaded). Top panels: (**a**) $-2\nabla \cdot \mathbf{Q}$ (shading) with $\mathbf{Q}$ vectors and (**d**) ω_{qg}. Middle panels: (**c**) Transverse components $-2\nabla \cdot \mathbf{Q}_n$ with $\mathbf{Q}_n$ vectors and (**e**) ω_n. Bottom panels: (**c**) Shearwise components, $-2\nabla \cdot \mathbf{Q}_s$ with $\mathbf{Q}_s$ vectors and (**f**) ω_s. In all panels the thin blue contours are the isentropes plotted at 2.5 K contour intervals, the thick blue contour is the 38 m s^{-1} 250 hPa isotach to highlight the located of the jet streak in Fig. 2 and the thinner solid (dashed) black closed curves are + 30 (- 30) gpm geopotential anomalies at 250 hPa. The composites shown are for $t = -24$ h

in Sect. 2.4. Figs 6a–c present the 700 hPa level $-2\nabla \cdot \mathbf{Q}$, $-2\nabla \cdot \mathbf{Q}_n$ and $-2\nabla \cdot \mathbf{Q}_s$ as shaded fields together with the associated vectors $\mathbf{Q}$, $\mathbf{Q}_n$ and $\mathbf{Q}_s$, respectively. The thin blue contours are the isentropes and the rest of the fields are as in the previous figures. The corresponding panels on the right show the ω_{qg}, ω_n and ω_s fields which were produced by means of $\omega_{qg} = L^{-1}(-2\nabla \cdot \mathbf{Q})$, $\omega_n = L^{-1}(-2\nabla \cdot \mathbf{Q}_n)$ and $\omega_s = L^{-1}(-2\nabla \cdot \mathbf{Q}_s)$ using the successive over-relaxation method of Park et al. (2021). Figure 6, 7 and 8 show composites of these fields for $t = -24$, 0 and + 24 hrs time lags, respectively.

Figure 6d, 7d and 8d show that ω_{qg} broadly captures the structure of ω shown in panels (a), (b) and (c) of Fig. 5, for time lags $t = -24$, 0 and + 24 h, respectively. The vertically upward motion is strong at the inflection point/area of the baroclinic wave and appears to extend into South Africa, where it is weaker. The fact that there is agreement between these and that the former is produced directly from the forcing $-2\nabla \cdot \mathbf{Q}$ (shown in Figs. 6a, 7a and 8a) means that we may use the decomposition of the forcing to further strengthen the argument presented in the previous section that the vertical motion over subtropical southern African is induced by the jet streak entrance dynamics found there rather than the divergence of the ageostrophic flow (right panels of Fig. 5).

We first consider the vectors at the jet entrance. As noted in Sect. 2.4, $|\mathbf{Q}_n| > |\mathbf{Q}_s|$ there, and this is evident by comparing Figs. 6b, c, 7b, c, and 8b, c which shows them for $t = -24$, 0, and +24 hrs, respectively. Also the $\mathbf{Q}_n$ vectors are oriented normal to the isentropes and pointing towards the warmer side of the domain, as expected (Keyser et al. 1992; Martin 2006; Park et al. 2021). They increase from the extratropics, maximise across the 325 K isentrope, or so, and then start decreasing north of that. This leads to regions of

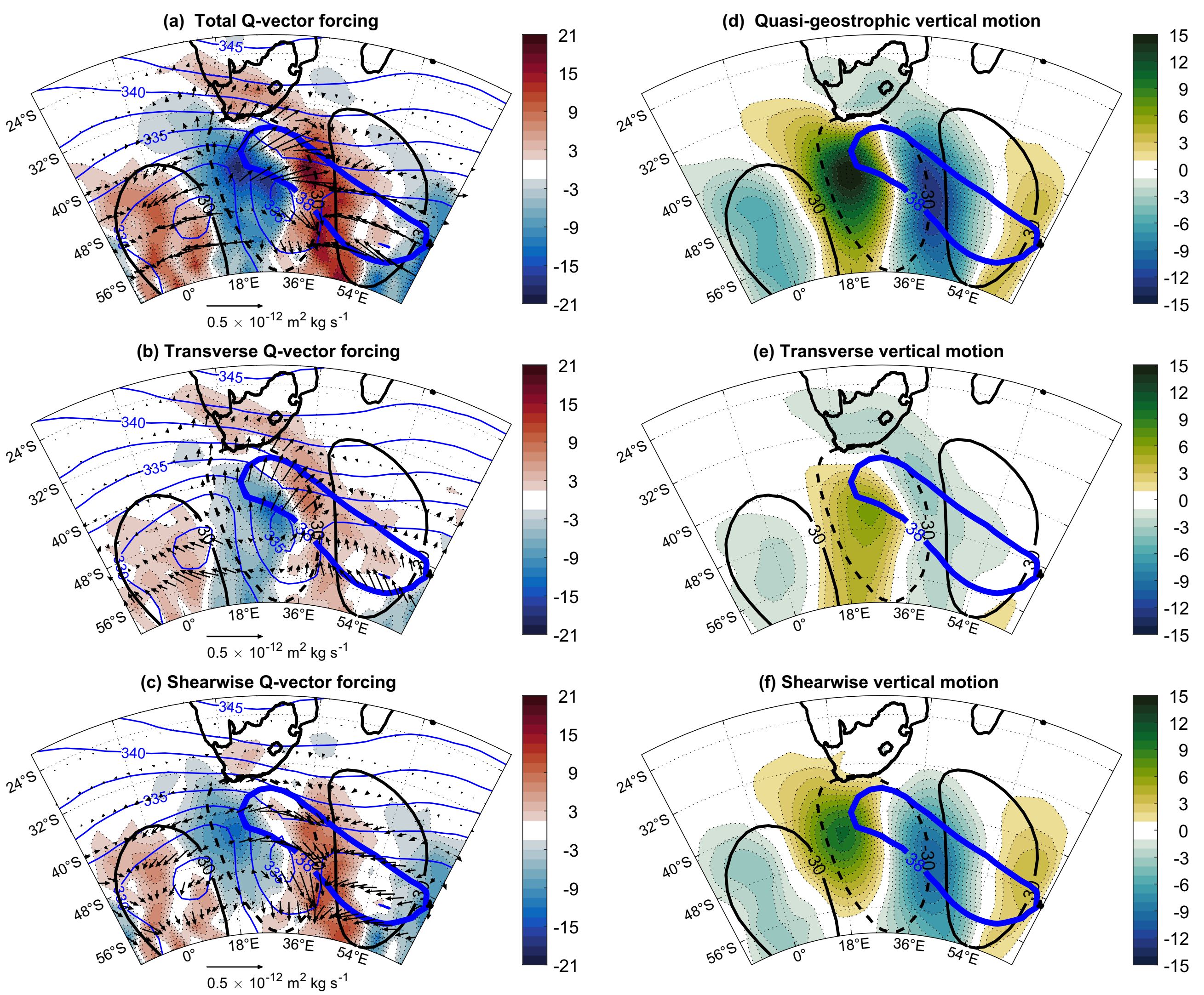

Fig. 7 Same as Fig. 6 but for time lag $t = 0$ h

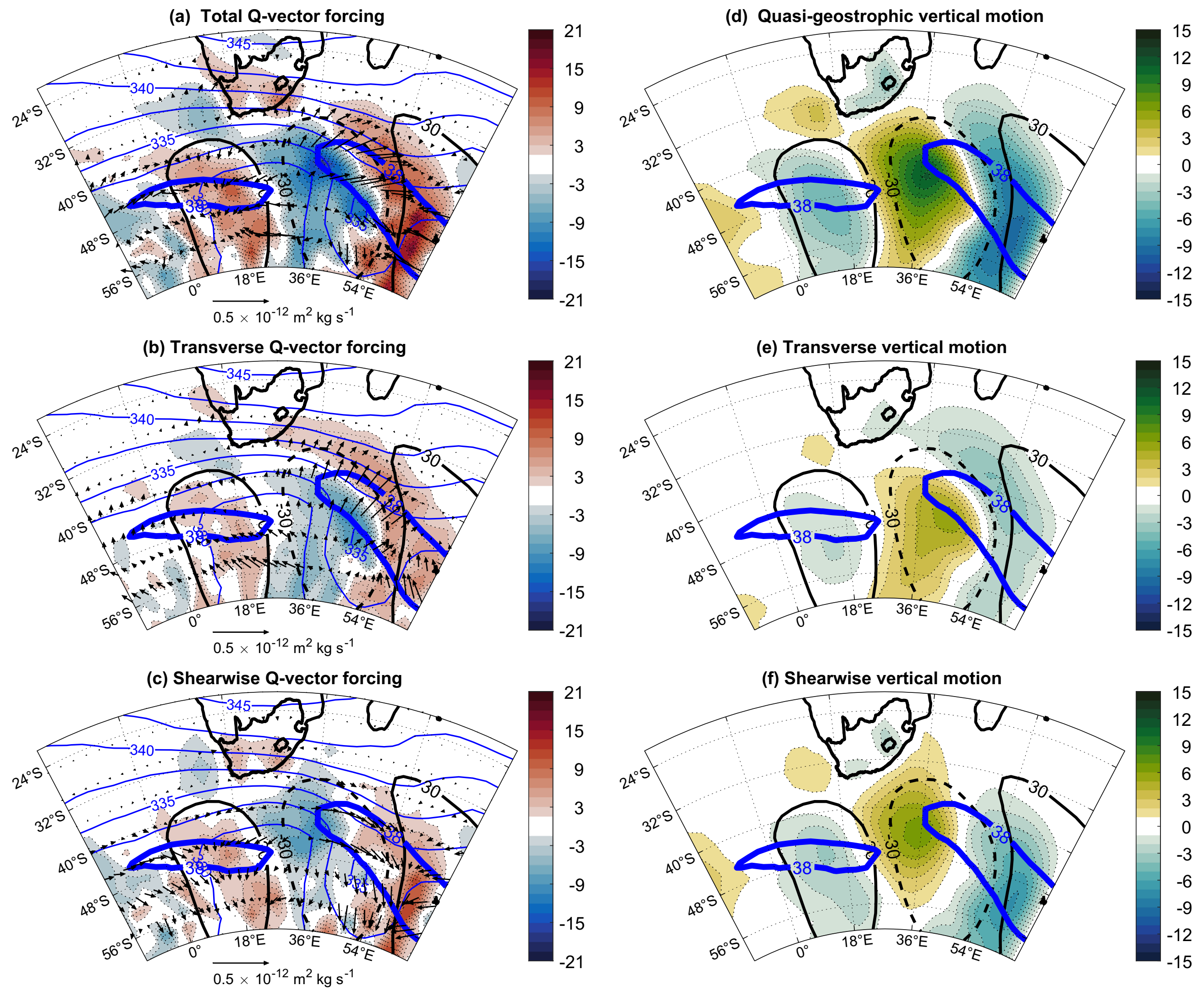

Fig. 8 Same as Fig. 6 but for time lag $t = +24$ h

$\nabla \cdot \mathbf{Q}_n < 0$ north of this isentrope including over the South African domain (where $-2\nabla \cdot \mathbf{Q}_n > 0$ in Fig 7b). By means of Eq. 3, this leads to $\omega_n < 0$, as seen in Figs. 6e, 7e and 8e. Sanders and Hoskins (1990); Simmonds and Keay (2000) did not decompose the **Q**-vector but the orientation of $\mathbf{Q}_n$ arrows is consistent with their findings so that the vertical motion experienced over South Africa is associated with the warm sector of the confluent flow at the jet entrance, as that study shows. This supports the discussion in Sect. 3.2 in which it was argued that vertical motion over the country is caused by the thermally direct circulation at the jet entrance in Fig. 3.

Again, as expected, the vectors $\mathbf{Q}_s$ are oriented tangentially to the isentropes and, more importantly in the context of this study, converge at the inflection point of the baroclinic wave, east of the upper level trough axis (Figs. 6c, 7c and 8c). This then induces ω_s (Figs. 6f, 7f and 8f), which dominates in the extra-tropics, approximately where $\nabla \cdot \mathbf{v}_a \approx \partial_x u_a$ dominates (right panels of Fig. 5); but certainly far from the land. So $\nabla \cdot \mathbf{Q}_s < 0$ implies $\omega_s < 0$ in the extratropics. Again Sanders and Hoskins (1990); Simmonds and Keay (2000) showed that the convergence of **Q**, which is dominated by $\mathbf{Q}_s$ in this study, induces vertical ascent there. The ω_n and ω_s fields produced here are structured as noted in Keyser et al. (1992), the former has a narrow banded structure that extends from southern Africa into the extratropics in a manner reminiscent of cloud bands associated with TTTs (Harrison 1984; Hart et al. 2023). ω_s has a circular wave scale structure (Keyser et al. 1992; Martin 2006, 2014; Park et al. 2021) and in the extratropic its values are an order of magnitude larger than those of ω_n. The situation over South Africa is reversed. ω_s is weak with values that are less than -0.01 Pa s^{-1}; whilst ω_n values are in excess of -0.2 Pa s^{-1}, meaning that ω_{qg} over South Africa is mostly caused by transverse circulation processes associated with the jet entrance. This further shows that vertically upward motion in the extratropics is caused by dynamical processes that different from those that cause it in subtropical southern Africa, in support of the qualitative argument presented in the previous section.

To further the argument presented above, following Hart et al. (2010), Fig. 9a, b show ω (contours) and its percentage (shaded) explained by (a) ω_n and (b) ω_s. Comparing the two panels suggest that the full vertical motion over the interior of South Africa is better explained by ω_n than by ω_s. There may be doubt about the validity of the quasi-geostrophic theory over the country, given its location so far north of the extra-tropics where the Rossby number is small but Fig. 9 indicates that the full observed omega is unlikely to be caused by the upper air divergence.

This Q-vector analysis therefore indicates the predominance of transverse over shearwise circulation in providing quasigeostrophic uplift over South Africa. It challenges the general view that upper-level divergence induces uplift for summertime precipitation over southern Africa. However, given the f-plane dry adiabatic assumptions of the QG-framework, this transverse circulation remains a partial explanation of the full uplift field. This is seen in Fig. 9 with no more that 40% of total uplift explained by ω_n as diabatic processes during convection likely amplify this vertical motion, as suggested in previous literature (e.g. Hart et al. 2010).

4 Discussion and concluding remarks

In this study the well-known westerly wave (Tyson and Preston-Whyte 2002) is considered to be a linear baroclinic wave that propagates eastward across southern African sector from the southeast South Atlantic into the southwest South Indian Oceans. Using ERA5 reanalysis data from 1979 to 2020, the only waves that were considered are associated with ridging high pressure systems. As stringent as this requirement seems, its purpose is to ensure that the westerly waves considered here could be associated with the transport of moisture onto land from the South West Indian Ocean. Composite analysis showed that the trough that actually impacts the South African domain develops over the South Atlantic Ocean and propagates into the South African domain as ridging occurs and then leaves the domain with the first 24 h of ridging. As it passes over the country, vertically upward motion occurs, which is replaced by downward motion over the southern and southeastern coast, once it has propagated further east into the southwest Indian Ocean.

Figure 10 shows a schematic diagram, visually summarising our findings. The curved yellow arrows represent the two prevailing jet streaks that materialise under the conditions of

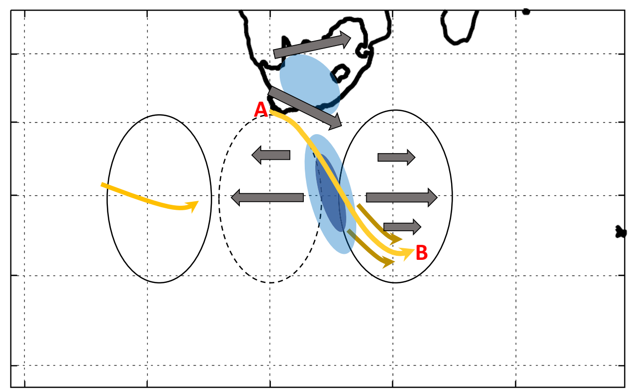

Fig. 10 Schematic summarising the synoptic scale processes discussed from Figs. 1, 2, 3, 4, 5, 6, 7 and to 8. The thin dashed and solid back oval shapes represent the negative and positive geopotential height anomalies, respectively. The straight grey arrows represent the ageostrophic flow, which induces vertical motion in the extratropics, represented by the blue colored oval shape. The thick curved yellow arrows represent the jet streaks, with two additional light brown shorter arrows representing the strength of the downstream jet (marked AB) at the bottom of the wave where the flow is supergeostrophic across the ridge axis. The jet streak is embedded in the baroclinic wave. There is weaker vertical motion over South Africa, flanked by two grey arrows representing the diffluent ageostrophic flow observed there

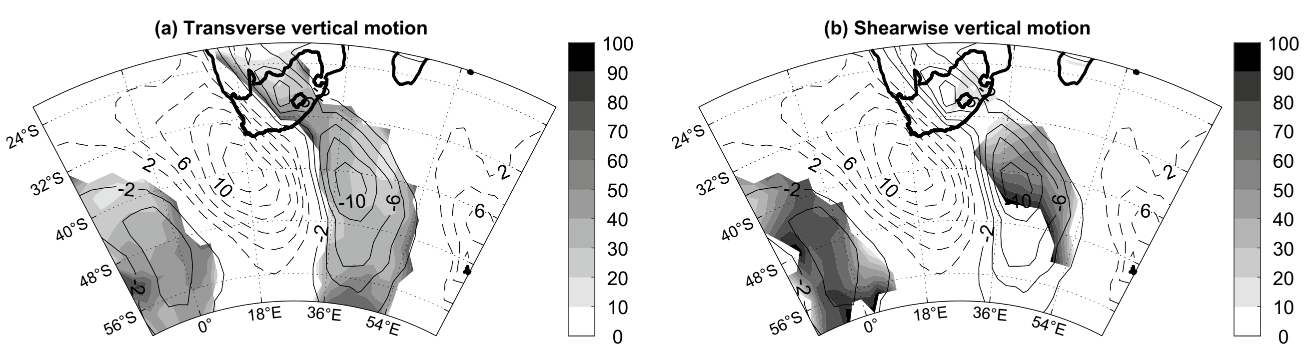

Fig. 9 Contours of ω plotted at 0.02×10^{2} Pa s^{-1} intervals with percentage of ω explained by **a** ω_n and **b** ω_s uplift (shaded) at time lag $t = 0$ h

ridging highs co-occurring with linear westerly waves, with the one downstream labelled AB. The shorter dark yellow curves near the label B at the bottom of the ridge represent the fact that this downstream jet streak is stronger, particularly close to the exit. This leads to the supergeostrophic flow found there. The grey arrows show the orientation of the ageostrophic flow, suggesting that under the circumstances of this study, it is divergent in the extratropics and diffluent over subtropical southern Africa. The vertical motion that occurs in the domain during the passage of a westerly trough is represented by the blue oval shapes in the schematic. It is stronger in the extra-tropics, as indicated by the darker blue shade, where the upper air divergence is strongest. The ageostrophic flow itself is zonal so the the divergence field is dominated by $\partial_x u_a$. Conventionally, one would assume that this extratropical upward motion field extends into South Africa and that which is found there is also caused by this upper air divergence field. We propose in this study that this is unlikely to be the case. Instead, air rises over the country as a result of the thermally direct transverse circulation at the entrance of the jet streak AB. To attest to this, the ageostrophic flow over the country is diffluent (see the orientation of the vectors), so that the divergence field found there is dominated by $\partial_y v_a$. This is consistent with Keyser and Shapiro (1986)'s cross-front geostrophy. The simplified continuity equation that results i.e. $\partial_y v_a + \partial_p \omega = 0$, meaning that the vertical motion over South Africa is caused by a behaviour of the ageostrophic flow that this dynamically different from the one observed in the extratropics i.e $\partial_y v_a$, instead of $\partial_x u_a$.

To the best of our knowledge, there is no theory free of quasi-geostrophic assumptions existing in the literature that would enable the decomposition of vertical motion in the South African domain as well as the one employed in this study. This is important to note here as the dynamics of South African weather are subtropical where quasi-geostrophic analysis might not be valid, but are intimately linked to extratropical processes where the quasi-geostrophic assumption is more valid. Be that as it may, ω_{qg} appears to be a reasonable approximation of ω in the domain, so that quasi-geostrphic theory maybe used to understand some aspects of the country's weather phenomena. Even as this is a limitation, this study has shown that the decomposition of the **Q**-vector forcing successfully separates vertical ascent over South Africa from that which occurs in the extratropics, at the inflection area of the westerly wave, east of the upper level trough axis. As noted above, the former is caused by the thermally direct circulation at the jet entrance, rather than by the divergence, in the extratropics. The decomposition of the **Q** vector forcing shows that, on the one hand the quasi-geostrophic vertical motion in the country is dominated by the transverse component of it, which is associated with the jet entrance because it is perpendicular to the isentropes and pointing towards the warm sector jet. On the other hand, the extratropical vertical motion field is dominated by the shearwise component of the **Q**-vector that converges where $\partial_x u_a > 0$ dominates. These findings are entirely consistent with Sanders and Hoskins (1990); Simmonds and Keay (2000).

Results from our study have implications for forecasting, because verification of model simulations and model improvements can be extended beyond the analysis of rainfall and temperature simulations, but also determine whether models can distinguish between dynamical processes in the extra-tropics compared to those in the subtropics. Models that can perform well in different parts of the globe do not yet exist which has resulted in physics suites being developed. A study like this that shows that the ascent mechanism is different in subtropics to the extra-tropics can help towards understanding some of the shortcomings in the models.

A key purpose of this paper is to explore firstly, the commonly accepted heuristic of upper-level divergence driving uplift over southern Africa and secondly, how far simple linear frameworks can go in explaining key regional dynamics. Although this heuristic seems to be qualitatively inaccurate for the first aspect, the linear framework proves remarkably useful for the second. Since the linear analysis presented here is insufficient to provide a full explanation of vertical motion over the region, future studies should aim to extend our work using numerical model experiments. These experiments will need to be carefully designed since models are unable to fully represent all the details of the topography and, in any case, need work such as that presented in our manuscript to be able to fully and meaningfully interpret the changes in dynamics.

Acknowledgements This work is part of a broader project that aims is to understand the underlying dynamical processes of the important synoptic systems in the South Atlantic Ocean/South Africa basin. The authors would like to the Water Research Commission (Grant number: C2020/2021-00653) for its support. NCGH acknowledges support from NERC grant NE/V011928/1 and a UKRI Future Leaders Fellowship MR/W011379/1. We are also very grateful to Dr. Chanil Parker and Prof Seok-Woo Son, Seoul National University, for providing us with the successive over-relaxation code used in the study. A heartfelt gratitude also goes out to the anonymous reviewers who constructively assessed the work.

Author Contributions TN and TSR conceptualised the research, performed the calculations and produced the plots. TSR calculated the various vertical omega fields using Park et al. (2021)'s successive over relaxation method and TN prepared the schematics Fig. 1 and Fig. 9 and prepared the first draft of the manuscripts. All the authors contributed to the analysis and reviewed the manuscript.

Funding Open access funding provided by University of Pretoria. This study has been supported by the Water Research Foundation (Grant number: C2020/2021-00653) of South Africa and it is part of a larger project that aims to understand the underlying dynamical processes of

important synoptic systems in the South Atlantic Ocean/South Africa basin.

Data availability All the data used in the study was obtained are the Fifth Generation European Centre for Medium-Range Weather Forecasts reanalysis (ERA5) can be obtained from https://www.ecmwf.int/en/forecasts/datasets/reanalysis-datasets/era5.

Declarations

Conflict of interest The authors neither have conflict of interest nor competing interests.

Ethical approval Not Applicable.

References

Akahori K, Yoden S (1997) Zonal flow vacillation and bimodality of baroclinic eddy life cycles in simple global circulation model. J Atmos Sci 54:2351–2361. https://doi.org/10.1175/1520-0469(1997)054<2349:ZFVABO>2.0.CO;2

Barnes MA, Ndarana T, Landman W (2021a) Cut-off lows in the southern Hemisphere and their extension to the surface. Clim Dyn 56:3709–3732. https://doi.org/10.1007/s00382-021-05662-7

Barnes MA, Turner K, Ndarana T, Landman WA (2021b) Cape storm: a dynamical study of a cut-off low and its impact on South Africa. Atmos Res 249:105290. https://doi.org/10.1016/j.atmosres.2020.105290

Barnes MA, Ndarana T, Landman W (2022) Stratospheric intrusion depth and its effect on surface cyclogenetic forcing: an idealized potential vorticity (PV) inversion experiment. Weather Clim Dyn 3:1291–1309. https://doi.org/10.5194/wcd-3-1291-2022

Brown TJ, Hall BL (1999) The use of t values in climatological composite analyses. J Clim 12:2941–2944. https://doi.org/10.1175/1520-0442(1999)012<2941:TUOTVI>2.0.CO;2

Cook C, Reason CJC, Hewitson BC (2004) Wet and dry spells within particularly wet and particularly dry summers in the South African summer rainfall region. Clim Res 26:17–31. https://doi.org/10.3354/cr026017

Crespo NM, da Rocha RP, Sprenger M, Heini Wernli (2021) A potential vorticity perspective on cyclogenesis over centre-eastern South America. Int J Climatol 41:663–678. https://doi.org/10.1002/joc.6644

D'Abreton PC, Lindesay JA (1993) Water vapour transport over southern Africa during wet and dry early and late summer months. Int J Climatol 13:151–170. https://doi.org/10.1002/joc.3370130203

Dyson L (2015) A heavy rainfall sounding climatology over Gauteng, South Africa, using self-organising maps. Clim Dyn 45:3051–3065. https://doi.org/10.1007/s00382-015-2523-3

Engelbrecht CJ, Landman WA, Engelbrecht FA, Malherbe J (2015) A synoptic decomposition of rainfall over the Cape south coast of South Africa. Clim Dyn 44:2589–2607. https://doi.org/10.1007/s00382-014-2230-5

Favre A, Hewitson B, Tadross M, Lennard C, Cerezo-Mota R (2012) Relationships between cut-off lows and the semiannual and southern oscillations. Clim Dyn 38:1473–1487. https://doi.org/10.1007/s00382-011-1030-4

Favre A, Hewitson B, Lennard C, Cerezo-Mota R, Tadross M (2013) Cut-off lows in the South Africa region and their contribution to precipitation. Clim Dyn 41:2331–2351. https://doi.org/10.1007/s00382-012-1579-6

Fuenzalida HA, Sánchez R, Garreaud RD (2005) A climatology of cutoff lows in the southern Hemisphere. J Geophys Res Atmos 110:1–10. https://doi.org/10.1029/2005JD005934

Gan MA, Piva ED (2013) Energetics of a southeastern Pacific cut-off low. Atmos Sci Let 14:272–280. https://doi.org/10.1002/asl2.451

Gan MA, Piva ED (2016) Energetics of a Southeastern Pacific cut-off lows. Clim Dyn 46:3453–3462. https://doi.org/10.1007/s00382-015-2779-7

Harangozo SA, Harrison MSJ (1983) On the use of synoptic data in indicating the presence of cloud bands over southern Africa. S Afr J Sci 79(10):413–414

Harrison MSJ (1984) A generalized classification of South African rain-bearing synoptic systems. Int J Climatol 4:547–560. https://doi.org/10.1002/joc.3370040510

Hart NCG, Reason CJC, Faucherau N (2010) Tropical-extratropical interactions over southern Africa: three cases of heavy summer season rainfall. Mon Wea Rev 138:2608–2623. https://doi.org/10.1175/2010MWR3070.1

Hart NCG, Reason CJC, Fauchereau N (2023) Cloud bands over southern Africa: seasonality, contribution to rainfall variability and modulation by the MJO. Clim Dyn 41:1199–1212. https://doi.org/10.1007/s00382-012-1589-4

Hersbach H, Bell B, Berrisford P, Hirahara S, Horanyi A, Munoz-Sabater J, Nicolas J, Peubey C, Radu R, Schepers D, Simmons A, Soci C, Abdalla S, Abellan X, Balsamo G, Bechtold P, Biavati G, Bidlot J, Bonavita M, De Chiara G, Dahlgren P, Dee D, Diamantakis M, Dragani R, Flemming J, Forbes R, Fuentes M, Geer A, Haimberger L, Healy S, Hogan RJ, Holm E, Janiskova M, Keeley S, Laloyaux P, Lopez P, Lupu C, Radnoti G, de Rosnay P, Rozum I, Vamborg F, Villaume S, Thepaut J-N (2020) The ERA5 global reanalysis. QJR Meteorol Soc 146:1999–2049. https://doi.org/10.1002/qj.3803

Holton JR, Hakim GJ (2014) An introduction to dynamic meteorology. In: 4th edn Elsevier Academic Press, pp 553. https://doi.org/10.1119/1.1987371

Hoskins BJ, Draghici I, Davies HC (1978) A new look at the ω-equation. Q J R Meteorol Soc 104:31–38. https://doi.org/10.1002/qj.49710443903

Hoskins BJ, McIntyre ME, Robertson AC (1985) On the use and significance of isentropic potential vorticity maps. QJR Meteorol Soc 111:877–946. https://doi.org/10.1002/qj.49711147002

Ivanciu I, Ndarana T, Matthes K, Wahl S (2022) On the ridging of the South Atlantic anticyclone over south Africa: the impact of Rossby wave breaking and of climate change. Geophys Res Lett 49:e2022GL099607. https://doi.org/10.1029/2022GL099607

James IN (1987) Suppression of baroclinic instability in horizontally sheared flows. J Atmos Sci 44:3710–3720. https://doi.org/10.1175/1520-0469(1987)044

James IN, Gray LJ (1986) Concerning the effect of surface drag on the circulation of a baroclinic planetary atmosphere. Quart J R Meteor Soc 112:1231–1250. https://doi.org/10.1002/qj.49711247417

Jones DA, Simmonds I (1993) A climatology of Southern Hemisphere extratropical cyclones. Clim Dyn 9:131–145. https://doi.org/10.1007/BF00209750

Kelbe B (1988) Features of westerly waves propagating over southern Africa during summer. Mon Weather Rev 116:60–70. https://doi.org/10.1175/1520-0493(1988)116<0060:FOWWPO>2.0.CO;2

Keyser D, Shapiro MA (1986) A review of the structure and dynamics of upper-level frontal zones. Mon Weather Rev 114:452–499. https://doi.org/10.1175/1520-0493(1986)114<0452:AROTSA>2.0.CO;2

Keyser D, Schmidt BD, Duffy DG (1992) Quasigeostrophic vertical motions diagnosed from along- and cross-isentrope components of the Q vector. Mon Weather Rev 120:731–741. https://doi.org/10.1175/1520-0493(1992)120

Kuete G, Pokam Mba W, Washington R (2020) African easterly jet south: control, maintenance mechanisms and link with Southern subtropical waves. Clim Dyn 54:1539–1552. https://doi.org/10.1007/s00382-019-05072-w

Lim GH, Holton JR, Wallace JM (1991) The structure of the ageostrophic wind field in baroclinic waves. J Atmos Sci 48:1733–1745. https://doi.org/10.1175/1520-0469(1991)048

Macron C, Pohl B, Richard Y (2014) How do tropical temperate troughs form and develop over southern Africa. J Clim 27:1633–5199. https://doi.org/10.1175/JCLI-D-13-00175.1

Martin JE (2006) The role of shearwise and transverse quasigeostrophic vertical motions in the midlatitude cyclone life cycle. Mon Weather Rev 134:1174–1193. https://doi.org/10.1175/MWR3114.1

Martin JE (2014) Quasi-geostrophic diagnosis of the influence of vorticity advection on the development of upper level jet-front systems. Q J R Meteorol Soc 140:2658–2671. https://doi.org/10.1002/qj.2333

McIntyre ME, Palmer TN (1983) Breaking planetary waves in the stratosphere. Nature 305:593–600. https://doi.org/10.1038/305593a0

Mendes D, Souza EP, Trigo IF, Miranda PMA (2007) On precursors of South American cyclogenesis. Tellus A: Dyn Meteorol Oceanogr 59:114–121. https://doi.org/10.1111/j.1600-0870.2006.00215.x

Moon W, Feldstein SB (2009) Two types of baroclinic life cycles during the Southern Hemisphere summer. J Atmos Sci 66:1401–1417. https://doi.org/10.1175/2008JAS2826.1

Moore JT, VanKnowe GE (1992) The effect of jet-streak curvature on kinematic fields. Mon Wea Rev 120:2429–2441. https://doi.org/10.1175/1520-0493(1992)120

Nakamura M, Plumb RA (1994) The effects of flow asymmetry on the direction of Rossby wave breaking. J Atmos Sci 51:2031–2045. https://doi.org/10.1175/1520-0469(1994)051<2031:TEOFAO>2.0.CO;2

Ndarana T, Waugh DW (2010) The link between cut-off lows and Rossby wave breaking in the Southern Hemisphere. QJR Meteor Soc 136:869–885. https://doi.org/10.1002/qj.627

Ndarana T, Bopape M, Waugh D, Dyson L (2018) The influence of the lower stratosphere on ridging Atlantic Ocean anticyclones over South Africa. J Clim 31:6175–6187. https://doi.org/10.1175/JCLI-D-17-0832.1

Ndarana T, Rammopo TS, Chikoore H, Barnes MA, Bopape M (2020) A quasigeostrophic diagnosis of cut-off low pressure systems over South Africa and surrounding ocean. Clim Dyn 55:2631–2644. https://doi.org/10.1007/s00382-020-05401-4

Ndarana T, Mpati S, Bopape M, Engelbrecht FA, Chikoore H (2021a) The flow and moisture fluxes associated with ridging South Atlantic Ocean anticyclones during the subtropical southern African summer. Int J Climatol 41:E1000–E1017. https://doi.org/10.1002/joc.6745

Ndarana T, Rammopo TS, Bopape M, Reason CJC, Chikoore H (2021b) Downstream development during South African cut-off pressure systems. Atmos Res 249:105315. https://doi.org/10.1016/j.atmosres.2020.105315

Ndarana T, Rammopo TS, Reason CJC, Bopape M, Engelbrecht FA, Chikoore H (2022) Two types of ridging South Atlantic Ocean anticyclones over South Africa and associated dynamical processes. Atmos Res 265:105897. https://doi.org/10.1016/j.atmosres.2021.105897

Ndarana T, Lekoloane LE, Rammopo TS, Reason Chris JC, CJC, Mary-Jane M. Bopape MM, Chikoore H, Engelbrecht FA (2023) Downstream development during ridging South Atlantic Ocean anticyclones. Clim Dyn. https://doi.org/10.1007/s00382-023-06717-7

Orlanski I, Sheldon J (1995) Stages in the energetics if baroclinic systems. Tellus 47A:605–628. https://doi.org/10.1034/j.1600-0870.1995.00108.x

Palmén E (1949) Origin and structure of high-level cyclones south of the maximum westerlies. Tellus 1:22–31. https://doi.org/10.1111/j.2153-3490.1949.tb01925.x

Palmén E, Newton C (1969) Atmospheric circulation systems. Academic Press, New York

Park C, Son S-W, Kim J-H (2021) Role of baroclinic trough in triggering vertical motion during summertime heavy rainfall events in Korea. J Atmos Sci 78:1687–1702. https://doi.org/10.1175/JAS-D-20-0216.1

Peters D, Waugh DW (1996) Influence of barotropic shear on the poleward advection of upper-tropospheric air. J Atmos Sci 53:3013–3031. https://doi.org/10.1175/1520-0469(1996)053<3013:IOBSOT>2.0.CO;2

Pinheiro HR, Hodges KI, Gan MA, Ferreira NJ (2017) A new perspective of the climatological features of upper-level cut-off lows in the Southern Hemisphere. Clim Dyn 48:541–559. https://doi.org/10.1007/s00382-016-3093-8

Pinheiro HR, Hodges KI, Gan MA, Ferreira SHS, Andrade KM (2022) Contributions of downstream baroclinic development to strong Southern Hemisphere cut-off lows. QJR Meteorol Soc 148:214–232. https://doi.org/10.1002/qj.4201

Reboita MS, da Rocha RP, Ambrizzi T, Ambrizzi T, Sugahara S (2010) South Atlantic ocean cyclogenesis climatology simulated by regional climate model (RegCM3). Clim Dyn 35:1331–1347. https://doi.org/10.1007/s00382-009-0668-7

Reboita MS, Ambrizzi T, Silva BA, Pinheiro RF, da Rocha RP (2019) The south Atlantic subtropical anticyclone: present and future climate. Front Earth Sci 7:8. https://doi.org/10.3389/feart.2019.00008

Reyers M, Shao Y (2019) Cut off lows off the coast of the atacama desert under present day condition and in the last glacial maximum. Global Planet Change 181:102–983. https://doi.org/10.1016/j.gloplacha.2019.102983

Sanders F, Hoskins BJ (1990) An easy method for estimation of Q-vectors from weather maps. Weather Forecast 5:346–353. https://doi.org/10.1175/1520-0434(1990)005

Simmonds I, Keay K (2000) Mean southern hemisphere extratropical cyclone behavior in the 40-Year NCEP-NCAR reanalysis. J Clim 13:873–885. https://doi.org/10.1175/1520-0442(2000)013

Sinclair MR (1995) A climatology of cyclogenesis for the Southern Hemisphere. Mon Wea Rev 123:1601–1619. https://doi.org/10.1175/1520-0493(1995)123

Singleton AT, Reason CJC (2006) Numerical simulations of a severe rainfall event over the Eastern Cape coast of South Africa: sensitivity to sea surface temperature and topography. Tellus A Dyn Meteorol Oceanogr 58:335–367. https://doi.org/10.1111/j.1600-0870.2006.00180.x

Singleton AT, Reason CJC (2007a) Variability in the characteristics of cut-off low pressure systems over subtropical southern Africa. Int J Climatol 27:295–310. https://doi.org/10.1002/joc.1399

Singleton AT, Reason CJC (2007b) A numerical study of an intense cut-off low pressure system over South Africa. Mon Wea Rev 135:1128–1150. https://doi.org/10.1175/MWR3311.1

Taljaard JJ (1985) Cut-off lows in the South African region. South African Weather Bureau Technical Paper 14, 153. [Available from the South African Weather Service, Private Bag x097, Pretoria, 0001, South Africa.]

Thoithi W, Blamey R, Reason CJC (2022) April 2022 Floods over East Coast South Africa: Interactions between a mesoscale convective system and a coastal meso-low. Atmosphere 14(1):78. https://doi.org/10.3390/atmos14010078

Thorncroft CD, Hoskins BJ, McIntyre ME (1993) Two paradigms of baroclinic-wave life-cycle behaviour. QJR Meteor Soc 119:17–55. https://doi.org/10.1002/qj.49711950903

Tyson PD, Preston-Whyte RA (2002) The weather and climate of southern Africa, 2nd edn. Oxford University Press, Cape Town

Vigaud N, Pohl B, Crétat J (2012) Tropical-temperate interactions over southern Africa simulated by a regional climate model. Clim Dyn 39:2895–2916. https://doi.org/10.1007/s00382-012-1314-3

Viljoen E, Dyson L, Moyo I (2023) Africánes in southern Africa: attributes and contribution to rainfall of a continental tropical low. Clim Dyn 60:1599–1617. https://doi.org/10.1007/s00382-022-06380-4